

Dissociative recombination, and vibrational excitation of CO^+ : model calculations and comparison with experiment

J. Zs Mezei^{1,2,3}, R. D. Backodissa-Kiminou¹, D. E. Tudorache^{1,4}, V. Morel⁵, K. Chakrabarti^{1,6}, O. Motapon⁷, O. Dulieu², J. Robert², W.-Ü. L. Tchang-Brillet⁸,

A. Bultel⁵, X. Urbain⁹, J. Tennyson¹⁰, K. Hassouni¹¹, and I. F. Schneider^{1,2*}

¹LOMC CNRS–Université du Havre–Normandie Université, 76058 Le Havre, France

²LAC, CNRS–Université Paris-Sud–ENS Cachan–Université Paris-Saclay, 91405 Orsay, France

³HUN-REN Institute for Nuclear Research (ATOMKI), H-4001 Debrecen, Hungary

⁴Lab. EM2C, CNRS–École Centrale Paris, 92295 Châtenay-Malabry, France

⁵CORIA CNRS–Université de Rouen–Université Normandie, F-76801 Saint-Etienne du Rouvray, France

⁶Dept. of Mathematics, Scottish Church College, Calcutta 700 006, India

⁷LPF, UFD Math., Info. Appliq. Phys. Fondamentale,

University of Douala, P. O. Box 24157, Douala, Cameroon

⁸LERMA, Observatoire de Paris, CNRS-Sorbonne Universités-UPMC Univ Paris 06, F-92195 Meudon, France

⁹Institute of Condensed Matter and Nanosciences, PAMO - Louvain-la-Neuve, 1348, Belgium

¹⁰Dept. of Physics and Astronomy, University College London, WC1E 6BT London, UK and

¹¹LSPM, CNRS–Université Paris 13–USPC, 93430 Villetaneuse, France

(Dated: May 13, 2024)

The latest molecular data - potential energy curves and Rydberg/valence interactions - characterizing the super-excited electronic states of CO are reviewed, in order to provide inputs for the study of their fragmentation dynamics. Starting from this input, the main paths and mechanisms for CO^+ dissociative recombination are analyzed; its cross sections are computed using a method based on Multichannel Quantum Defect Theory. Convolutated cross sections, giving both isotropic and anisotropic Maxwellian rate-coefficients, are compared with merged-beam and storage-ring experimental results. The calculated cross sections underestimate the measured ones by a factor of 2, but display a very similar resonant shape. These facts confirm the quality of our approach for the dynamics, and call for more accurate and more extensive molecular structure calculations.

PACS numbers: 33.80. -b, 42.50. Hz

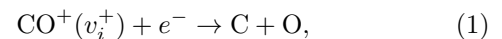
I. INTRODUCTION

Carbon monoxide (CO) is the most abundant molecule detected in the interstellar medium after molecular hydrogen, and being heteronuclear is much easier to be detected in emission. Its observation at long wavelengths, as in radio astronomy, is the source of the much of the information obtained on different interstellar environments, from molecular clouds in which protostars form and irradiate the surrounding residual material, to the circumstellar disks that surround stars at the end of their lives and to the cometary gases. Its spectrum has been intensively studied in astrophysical context, since its large binding energy implies that many electronically excited states possess discrete line spectra, see [1–4] and references therein. In all cases, under the influence of ultraviolet radiation produced during the stellar cycle, CO is the subject of a rich photochemistry, implying the formation among other species, of its cation, CO^+ .

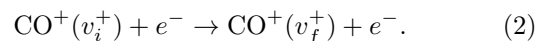
CO^+ was the first molecular ion discovered outside the Earth [5], has been identified as a major constituent of dense interstellar molecular clouds [6]. CO^+ also occurs in flames [7–9], and is expected to be very abundant in the plasmas formed by the hypersonic entry of spacecrafts and comets in the Martian atmospheres [10, 11]. Cold plasmas containing a large number of molecules and

molecular ions constitute a subject of rising scientific interest, involving more and more technological applications. CO^+ is of the most important of such molecular ionic species, since it occurs in practically all air assisted processes. Its dissociative recombination (DR) can be regarded as the main photochemical carbon loss process from the Martian atmosphere [12] and it is considered the major source of excited $\text{C}(^1D)$ atoms.

The kinetic description of all the above mentioned environments requires a good knowledge of the rate coefficients of the dominant reactions, including those between electrons and molecular ions. As for the CO^+ ions, their abundance is strongly affected by the DR,



but also by other related competitive processes, such as the *inelastic* ($v_f^+ > v_i^+$) and the *superelastic* ($v_f^+ < v_i^+$) collisions with electrons:



Here v_i^+ and v_f^+ stand for the initial and final vibrational quantum number of the target ion, and rotational structure was neglected.

The pioneering theoretical study of the DR rate coefficient made by [13] shows that the dominant routes for the DR process are curves of the $^3\Pi$, $^1\Pi$ and $^1\Sigma^+$ symmetries. Guberman calculated the rate constants at 300

*ioan.schneider@univ-lehavre.fr

K to be 4.2×10^{-7} cm³/s for $^{12}\text{C}^{16}\text{O}^+$ and 2.9×10^{-7} cm³/s for $^{13}\text{C}^{16}\text{O}^+$ respectively. The most recent storage ring experiments of [1] gave a rate coefficient of 2.75×10^{-7} cm³/s for $^{13}\text{C}^{16}\text{O}^+$ which is in good agreement with the calculations of Guberman. The earlier afterglow experiments [14] for $^{12}\text{C}^{16}\text{O}^+$ gave a rate coefficient of 1.6×10^{-7} cm³/s, which does not agree with the theoretical calculations for $v_i^+ = 0$ and may indicate that a proportion of the CO^+ in that experiment was vibrationally excited.

Recently, a series of *ab initio* calculations of the CO states relevant to DR (and of the couplings between them) have been performed by Chakrabarti and Tenynson [2, 3] using the *R*-matrix method. The data obtained makes a new Multichannel Quantum Defect Theory (MQDT) investigation of the process over the whole energy range explored by the experiments [1, 9] possible.

The main goal of the present work is to evaluate the DR cross sections and the thermal rate using the previously mentioned *ab initio* data of [2, 3]. The paper is structured in the following way: Section II outlines the main ideas and steps of our MQDT approach. Section III presents the molecular data used in the calculation. The main results are given in section IV and the paper ends by conclusions.

II. THE MQDT-TYPE APPROACH TO DR

The MQDT approach [15–18] has been shown to be a powerful method for the evaluation of the cross sections of the DR process. Although it was applied with a great success to several diatomic systems like H_2^+ and its isotopologues [19–24], O_2^+ [25, 26], NO^+ [27–29] and triatomics like H_3^+ [30–32], its application to vibrational transitions, mainly to superelastic collisions for NO^+ is relatively recent [33, 34].

We aim to describe the sensitivity of the reactive electron-cation collisions on the *vibrational* levels involved. At least to a first approximation, rotational effects are known to be negligible for CO^+ [28]. The reasons for this rely on the weak Rydberg-valence interaction responsible for the indirect process: since the rotational structures and interactions play their role especially within the indirect mechanism - due to its resonant character - the weakness of this latter process implies that the rotational effects - if of any relevance - can be roughly restricted to the existence of the centrifugal barrier, due to the rotational excitation. But even in this latter context, rotation does not matter very much, since the target ion and the neutral are *equally* excited and, consequently, the Franck-Condon overlaps (direct process) do not change significantly with respect to those occurring for the case of rotationally ground states. However, this does not mean that electron-impact rotational excitation is negligible [35].

The theoretical summary given below is limited to an account of the *vibrational* structure and coupling, illustrated mainly for DR. However, the reader should keep in mind that the other competitive reactions – such as

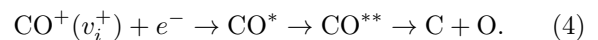
superelastic collision (SEC) ($v_i^+ > v_f^+$ in eq. (2)), *elastic collision* (EC) ($v_i^+ = v_f^+$) and *inelastic collision* (IC) ($v_i^+ < v_f^+$) – also occur and can display quite similar features.

The DR can take place following two mechanisms:

- (i) the *direct* process where the capture takes place into a dissociative state of the neutral system (CO^{**}),



- (ii) the *indirect* process where the capture occurs *via* a Rydberg state of the molecule CO^* which is predissociated by the CO^{**} state,



We note here, that we follow the standard nomenclature in this work, namely CO^{**} and CO^* represent the doubly excited and singly excited states of CO respectively. In both these processes autoionization is in competition with the predissociation and leads, through the reaction (2), to SEC, EC or IC.

The MQDT treatment of DR involves ionization channels (describing the electron-ion scattering) and dissociation channels (describing the atom-atom scattering). Each ionization channel consists of a Rydberg series of excited states, extrapolated above the continuum threshold - a vibrational level v^+ of the molecular ion. A channel is considered *open* if its corresponding threshold is situated *below* the total energy of the system, and *closed* in the opposite case. In the present work we have $N^+ = N$, and as for the dissociative channels, only open channels are used.

The present MQDT approach is based on a description of molecular states in which only part of electronic Hamiltonian is diagonalized, within subspaces of electronic states with similar nature. Moreover we use a quasidead representation of molecular states [36] to cope with problems due to the avoided crossings of the potential energy curves. The short-range electronic interactions between states of different subspaces are then represented in terms of an electronic coupling operator \mathcal{V} given by

$$\mathcal{V}_{d_j,lv}^\Lambda(E', E) = \langle \chi_{d_j}^\Lambda(R) | V_{d_j,l}^\Lambda(R) | \chi_v^\Lambda(R) \rangle, \quad (5)$$

which couples the ionization channels (labeled by lv) to the dissociative channels (labeled by d_j). Starting from \mathcal{V} , one can build the short-range reaction matrix \mathcal{K} , which is a solution of the Lippmann-Schwinger integro-differential equation:

$$\mathcal{K} = \mathcal{V} + \mathcal{V} \frac{1}{E - \mathbf{H}_0} \mathcal{K}. \quad (6)$$

\mathbf{H}_0 being the zeroth order Hamiltonian associated to the molecular system, i.e. the Hamiltonian operator excluding the interaction potential \mathbf{V} . The short-range effects are valid in the region of small electron-ion and nuclei-nuclei distances, namely in the ‘A-region’ [37] where the Born-Oppenheimer representation is appropriate for the description of the colliding system. Here, the energy-dependence of the electronic couplings can be neglected. In the case of weak coupling, a perturbative solution of equation (6) can be obtained. This solution has been proved to be exact to second order, in the case of energy-independent electronic couplings [38]. In the external zone, the ‘B-region’ [37] represented by large electron-core distances, the Born-Oppenheimer model is no longer valid for the ionization channels and a close-coupling representation in terms of ‘molecular ion + electron’ is more appropriate. This corresponds to a frame transformation defined by the projection coefficients:

$$\mathcal{C}_{lv^+, \Lambda\alpha} = \sum_v U_{lv, \alpha}^\Lambda \langle \chi_{v^+} | \cos(\pi\mu_l^\Lambda(R) + \eta_\alpha^\Lambda) | \chi_v^\Lambda \rangle, \quad (7)$$

$$\mathcal{C}_{d_j, \Lambda\alpha} = U_{d_j \alpha}^\Lambda \cos \eta_\alpha^\Lambda, \quad (8)$$

$$\mathcal{S}_{lv^+, \Lambda\alpha} = \sum_v U_{lv, \alpha}^\Lambda \langle \chi_{v^+} | \sin(\pi\mu_l^\Lambda(R) + \eta_\alpha^\Lambda) | \chi_v^\Lambda \rangle, \quad (9)$$

$$\mathcal{S}_{d_j, \Lambda\alpha} = U_{d_j \alpha}^\Lambda \sin \eta_\alpha^\Lambda. \quad (10)$$

Here, χ_{v^+} is the vibrational wavefunction of the molecular ion, and χ_v^Λ is a vibrational wavefunction adapted to the interaction (A) region. The index α denotes the eigenchannels built through the *diagonalization* of the reaction matrix \mathbf{K} in equation (6) and $U_{lv, \alpha}^\Lambda$ and η_α^Λ are related to the corresponding eigenvectors and eigenvalues, while Λ refers to the electronic symmetry of the neutral species ($^1\Sigma^+$, $^1\Pi$, and $^3\Pi$ in the present study).

The projection coefficients shown in (7)-(10) include the two types of couplings controlling the process: the *electronic* coupling, expressed by the elements of the matrices \mathbf{U} and $\boldsymbol{\eta}$, and the *non-adiabatic* coupling between the ionization channels, expressed by the matrix elements involving the quantum defect μ_l^Λ . This latter interaction is favored by the variation of the quantum defect with internuclear distance R . The matrices \mathcal{C} and \mathcal{S} with the elements given by (7) to (10) are the building blocks of the ‘generalized’ scattering matrix \mathbf{X} :

$$\mathbf{X} = \frac{\mathcal{C} + i\mathcal{S}}{\mathcal{C} - i\mathcal{S}}, \quad (11)$$

whereas the ‘proper’ scattering matrix, restricted to the *open* channels, is given by [16]:

$$S = \mathbf{X}_{oo} - \mathbf{X}_{oc} \frac{1}{\mathbf{X}_{cc} - \exp(-i2\pi\nu)} \mathbf{X}_{co}. \quad (12)$$

More precisely the physical S-matrix is obtained from the 2×2 sub-matrices of \mathbf{X} involving the open (o) and closed

(c) channels, and from the diagonal matrix $\boldsymbol{\nu}$ containing the effective quantum numbers $\nu_{v^+} = [2(E_{v^+} - E)]^{-1/2}$ (in atomic units) associated with each vibrational threshold E_{v^+} of the ion situated *above* the current energy E . For a molecular ion initially in vibrational level v_i^+ and recombining with an electron of energy ε , the cross section for capture into *all* the dissociative states d_j of the same symmetry Λ is given by:

$$\sigma_{\text{diss} \leftarrow v_i^+}^\Lambda = \frac{\pi \rho^\Lambda}{4\varepsilon} \sum_j \sum_l |S_{d_j \leftarrow lv_i^+}^\Lambda|^2, \quad (13)$$

where ρ^Λ is the ratio between the multiplicities of the neutral system and of the ion. One has to perform the MQDT calculation for each group of dissociative states of symmetry Λ , and the sum over the resulting cross sections is the total DR cross section:

$$\sigma_{\text{diss} \leftarrow v_i^+} = \sum_\Lambda \sigma_{\text{diss} \leftarrow v_i^+}^\Lambda \quad (14)$$

In a similar way, the cross section for a vibrational transition of a molecular ion from the initial level v_i^+ to the final level v_f^+ is (excitation and/or deexcitation):

$$\sigma_{v_f^+ \leftarrow v_i^+}^\Lambda = \frac{\pi \rho^\Lambda}{4 \varepsilon} \sum_{l, l'} |S_{l' v_f^+ \leftarrow l v_i^+}^\Lambda|^2, \quad (15)$$

while the total cross section for this vibrational transition reads as:

$$\sigma_{v_f^+ \leftarrow v_i^+} = \sum_\Lambda \sigma_{v_f^+ \leftarrow v_i^+}^\Lambda. \quad (16)$$

III. MOLECULAR DATA

A. *Ab initio* R-matrix calculations

The earliest attempts to compute excited states of CO relevant for the dissociative recombination and their autoionization widths goes back to 1996 [39, 40] but were restricted to a single geometry.

Ten years later, two of us [2, 3] performed a much more detailed R-matrix calculation for a series of fixed geometries. These calculations used up to the 14 lowest CO^+ states in a close coupling expansion where each of these states were represented using a valence complete active space configuration interaction expansion. The calculations were repeated for 10 different internuclear distances in the range of $1.5 a_0$ to $3.5 a_0$. Moreover [3] computed positions and widths for a number of dissociative states, which appear as resonances in the R-matrix scattering calculations, as a function of geometry. In particular, resonance states of electronic symmetry $^1\Sigma^+$, $^1\Pi$ and $^3\Pi$ that have been used in the present work as the other symmetries are only very weakly coupled.

Although the R-matrix resonance calculations [3] for the CO molecule have not been subject to comparisons

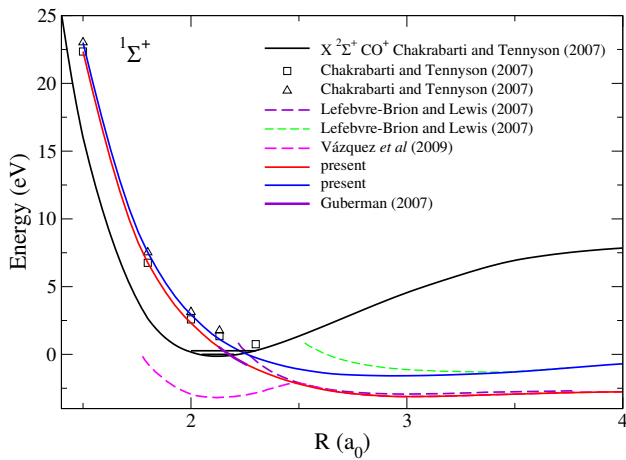


FIG. 1: Electronic states relevant for dissociative recombination with $^1\Sigma^+$ total symmetry. The ion ground state is shown in black; \square , \triangle are the R-matrix data [3]: (Chakrabarti and Tennyson 2007) for the lowest two CO^{**} states. The two continuous colored curves crossing the ion are the dissociative states obtained as outlined in section III B. The curves indicated in the legends refer to the curves from [13]: Guberman (2007), [42]; Lefebvre Brion and Lewis (2007) and [43]: Vazquez *et al* (2009)

and calibrations against all available spectroscopic data, some Rydberg states previously were calculated [2, 39]. It was found that these Rydberg states are placed higher than the observed values which is consistent with the variational nature of the R-matrix calculations. As a consequence, for low ℓ values, the estimated quantum defects were uniformly lower by about 0.07 compared to the available experimental data, see for example Tables 4 and 5 in [2]. The geometry dependent study on CO also showed that the quantum defects depend weakly on geometry except when the adiabatic curves are perturbed by an avoided crossing. This approach was successfully used by [29] to give greatly improved results for DR of NO^+ .

B. Modeling of the dissociative curves

The DR cross section is extremely sensitive to the position of the potential energy curves (PECs) of the neutral dissociative states with respect to that of the target ion. More specifically, a slight change of the crossing point of the PEC of a neutral dissociative state with that of the ion ground state can lead to a significant change in the predicted DR cross section. The magnitude of this change is roughly proportional to the square of the Franck-Condon type integral appearing in equation (5). This is an important issue here as we use the approximate PECs of the dissociative states above the ion ground state produced by R-matrix calculations [2, 3]. Indeed, for example, the crossing point of the lowest relevant $^1\Sigma^+$ state was found to be at higher energy and at larger internuclear distance than those obtained previously using a de-perturbation procedure [41] or *ab-initio* quantum chem-

istry computations [13]. Moreover, recent calculations [42–44] give PECs for the *lowest* neutral states relevant for DR, that only partially agree with those of the other calculations mentioned above.

All the available lower dissociative neutral states for the $^1\Sigma^+$ symmetry is shown in Figure 1, where we have presented the PECs relevant for the present study. The zero of energy was chosen to be the lowest vibrational level of the ground electronic state of the molecular ion. At the same time, apart from the dissociative curves, the MQDT calculation also requires the couplings between the ion ground state and the neutral dissociative states. The R-matrix calculations of [3] systematically provide autoionization widths for a large number of states which contain information about the required couplings. Such comprehensive data on couplings are not available from any other source. Thus use their data in our dynamical study on DR but correct the PECs when it is needed. In this way we undertake a semi-empirical calculation.

The dissociative (valence) states produce numerous avoided crossings when crossing the series of Rydberg states. By turning to the diabatic representation these avoided crossings will become "true" crossings essential for the *indirect* process. A quasi-diabatic PEC may be constructed, by smoothly connecting the resonant states obtained by scattering calculations to the asymptotic adiabatic states. A more detailed inspection of the available material, both diabatic and adiabatic, confirms the quality of the diabatic states obtained by [13], justifying their use in the construction of quasi-diabatic PECs by matching them in the relevant range of internuclear distances. As a general rule, we apply a slight shift to the R-matrix PECs only if it is necessary in order to match them with the diabatic curves of [13]. This is clearly the case for the first state of $^1\Sigma^+$ symmetry, see Fig 1. No such a behavior is visible for the second dissociative PEC, but we apply the same shift in quantum defect as we applied to connect the first state to its quasi-diabatic counterpart. Correlation to the proper asymptotic limits follows both the [45] rules and the adiabatic curves of [43], where they are available. In our model, we construct the lowest dissociative states as a function of the internuclear distance on the basis of a physically reasonable compromise between the available valence curves coming from all the above cited authors. As an example, consider the lowest state of $^1\Sigma^+$ symmetry: At the smaller internuclear distances, our quasi-diabatic PEC follows the R-matrix points of [3]. At larger internuclear distances we shift progressively the R-matrix dissociative curve in order to match them with those of [13]. This curve is used until it crosses the PEC of the molecular ion, and beyond, followed by a smooth connection to the lowest *diabatic* PEC of [42], which agrees very well with the asymptotic behavior of the lowest *adiabatic* potential energy curves of Vazquez at large internuclear distances. The dissociative curves constructed in this way will agree well with the PEC used by Guberman. A similar procedure is followed for all the other excited states with different symmetries.

As for the highest R-matrix dissociative PECs, we believe that they are robust, since the inherent errors in the R-matrix calculations decrease significantly within

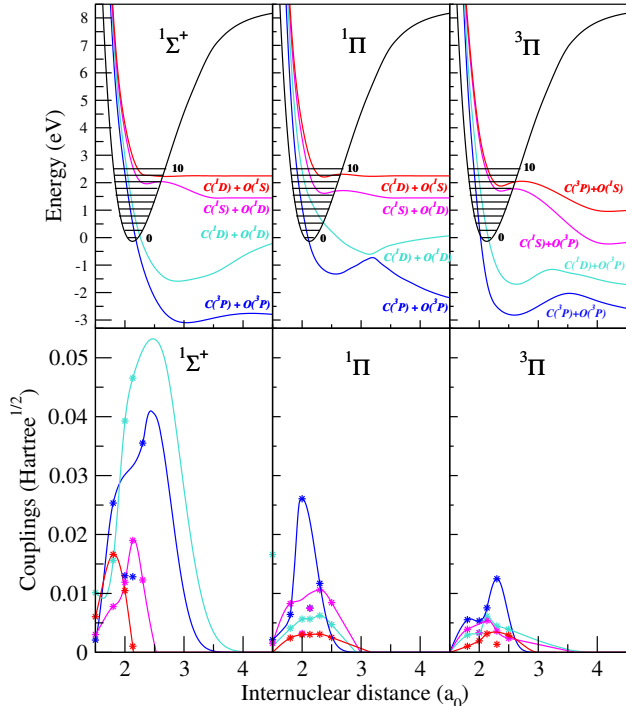


FIG. 2: The dissociative curves and couplings relevant for CO^+ dissociative recombination for the symmetries indicated in each figure. Top panel: the adjusted potential energy curves (cf section III), the ion ground state and first 10 vibrational levels are represented in black. Bottom panel: couplings between the valence dissociative states and the ionization continua.

the degree of excitation. Finally, Figure 2 shows the ion ground state and vibrational levels, the adjusted dissociative curves used in the present calculations and their corresponding autoionization widths coming from the R -matrix computations.

IV. EVALUATION OF THE CROSS SECTION USING THE MQDT-TYPE APPROACH

A. Mechanisms and couplings

Using the set of molecular data (PEC and electric couplings) determined as described in the previous section, we performed a series of MQDT calculations of the DR cross section, assuming the molecular ion to be initially in its electronic ground state ($X^2\Sigma^+$, $v_i^+ = 0, 1, 2$) and by neglecting rotational and spin-orbit effects. The calculations were performed for the states with total symmetry of $^1\Sigma^+$, $^1\Pi$ and $^3\Pi$, while the number of dissociative states considered for each symmetry are indicated in Figure 2.

We consider incident electron energies from 0.01 meV up to 3 eV. Since the dissociation energy of $\text{CO}^+(X^2\Sigma^+)$ is about 8.5 eV, the majority of the 53 vibrational levels

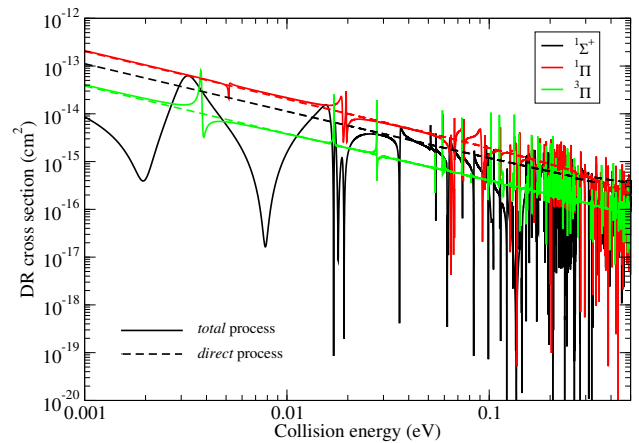


FIG. 3: Cross sections for the direct (dashed lines) and the total (direct + indirect) processes (continuous lines), for a vibrationally relaxed target in electronic states with $^1\Sigma^+$ (black), $^1\Pi$ (red) and $^3\Pi$ (blue) symmetries.

of the ion lie *above* the total energy of the $\text{CO}^+ + e$ system. These levels are associated with *closed* ionization channels, as defined in section II, responsible for temporary resonant capture into Rydberg states. As the energy increases, more and more ionization channels become *open*, which can result in autoionization leading to competitive processes like IEC or SEC, decreasing the flux of DR.

The direct electronic couplings between ionization and dissociation channels - equation (5) - have been extracted from the autoionization widths of the valence states [3].

Since a highly accurate solution of the Lippman-Schwinger system of integral equation (6) is difficult to obtain [46, 47], we take advantage of the fact that the couplings (among ionization and dissociation channels) involved are small and perturbative solution is acceptable. Following the main ideas of the earlier studies [20, 25], we adopt a second-order perturbative expansion, which accounts for all the basic mechanisms involved in DR, including *indirect* electronic interaction between the ionization channels.

The non-adiabatic couplings between the ionization channels rely, see Eqs. (7) and (8), on the R dependence of the quantum defects, which have been evaluated using the *ab initio* calculations described in Section III A.

For each dissociative channel available, we have considered its interaction with the most relevant series of Rydberg states, namely for $^1\Sigma^+$ symmetry the lowest 4 partial waves (s , p , d and f) were considered, while for the $^1\Pi$ and $^3\Pi$ symmetries only the lowest 3 (s , p , d) have been used. For the sake of simplicity, figure 2 shows the so-called global couplings which were constructed using the autoionization widths of [2, 3], namely

$$V_{d_j}^\Lambda = \left(\left(\sum_l \Gamma_{d_j,l}^\Lambda \right) / 2\pi \right)^{1/2}.$$

According to Eq. (12), the interference between the *direct* process (involving open channels exclusively and described by the first term: \mathbf{X}_{oo}) and the *indirect* one (involving closed as well as open channels and accounted for by the second term) results in what the *total* process.

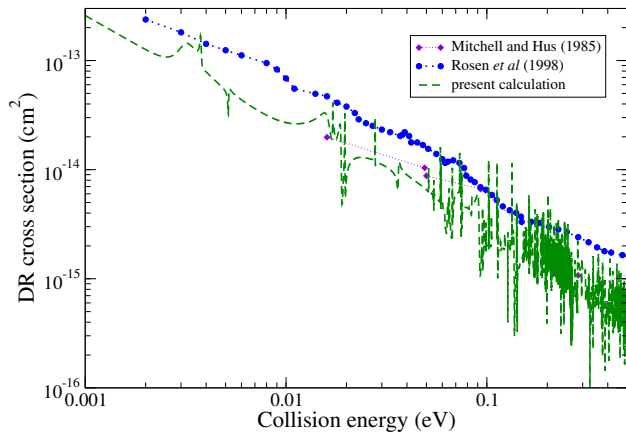


FIG. 4: Cross sections for the total (direct + indirect) DR process for a vibrationally relaxed target including the summed-up contributions of the states with $^1\Sigma^+$, $^1\Pi$ and $^3\Pi$ symmetry. The experimental results of [9] are shown with a dotted line with full violet diamonds, while those of [1] with dotted line with full blue circles, respectively.

The role of the direct and indirect mechanisms in the DR process can be seen in figure 3. The full colored lines show the total cross sections for the different symmetries used in the calculations, while dashed lines of the same color represent the cross sections given by the direct process only. As one could expect from the magnitude of the valence-Rydberg couplings, see figure 2, a strong dependence on the states and interactions can be observed, the majority of the cross section is given by the $^1\Pi$ and $^1\Sigma^+$ symmetries, while the $^3\Pi^+$ symmetry contributes only a small part. Moreover, for both states with Π symmetry, the indirect process plays a minor role for this ion; the magnitude of the total cross section is given by the direct process and the indirect one is responsible for the resonance structures. This is most striking for the $^1\Pi$ symmetry, where the total and direct only cross sections lie on the top of each other. The importance of the indirect mechanism is relevant for the $^1\Sigma$ symmetry, where due to the *destructive* interference between the direct and indirect processes the total cross section is lowered by almost one order of magnitude compared to the direct one, at certain collision energies. The indirect processes give rise to broad resonance structures in the range of the collision energy of the present study. Even though the indirect process globally plays a minor role, evaluating its effect gives increased insight into the recombination mechanism.

The importance of the different dissociation paths in our calculation is summarized in table I. Our calculated final state distribution are compared with the experimental values of [1] for four relative collision (detuning) energies. For the zero collision energy the statistical error was evaluated to be about 5%, while for higher energy values, due to the poor statistics, it is around 30%.

The dominant dissociation pathway for the DR of the CO^+ is the one which correlates with the $\text{C}(^3\text{P})+\text{O}(^3\text{P})$ atomic limits. Table I shows a qualitative agreement between the calculated and the measured final state dis-

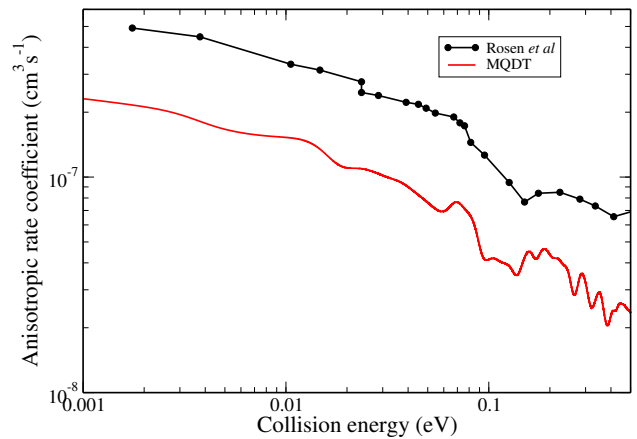


FIG. 5: Anisotropic rate coefficients for a vibrationally relaxed target. Experimental results [1] are in given in black with filled circles. Our theoretical results, for all symmetries considered here, are shown in red.

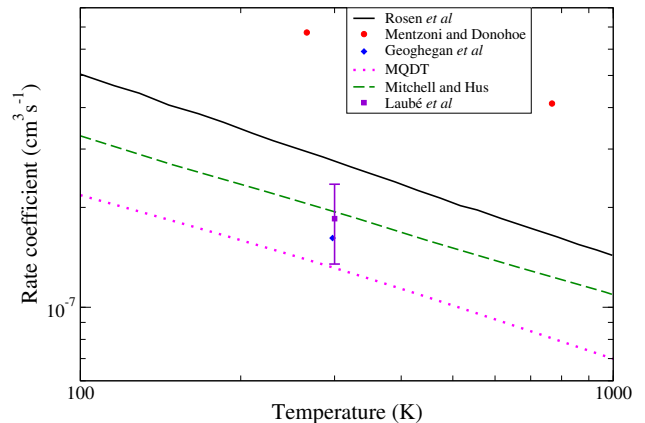


FIG. 6: Isotropic rate coefficients for a vibrationally relaxed target. Our theoretical results, for all symmetries considered here, are represented by magenta dotted line. The experimental results are shown as follows: [9], green dashed line; [1], black solid line; [14], blue diamonds, [48], red circles and [49], violet squares.

tributions. The agreement is good, particularly at low collision energies. At higher energies, the two sets of data disagrees, mainly due to the increased experimental statistical errors and the fact that our model lacks a dissociating pathway correlating to the $\text{C}(^3\text{P})+\text{O}(^1\text{D})$ atomic limits.

V. RESULTS AND DISCUSSION

The DR cross section corresponding to the three symmetries contributing to the process ($^1\Sigma^+$, $^1\Pi$ and $^3\Pi$), summed according to Eq. (14), are shown in figure 4. The calculations have been performed for the $^{12}\text{C}^{16}\text{O}^+$ isotopologue of the cation. The total cross section is characterized by resonance structures, superimposed on a smooth background (*direct* process only). The strong

TABLE I: The calculated final state distribution and its comparison with the experimental values for four relative collision (detuning) energies.

Dissociation path	energy (eV)							
	10^{-5}		0.4		1		1.5	
	calc	exp [†]	calc	exp	calc	exp	calc	exp
C(³ P)+O(³ P)	86.56%	76.1%	80.85%	53%	43.25%	39%	50.93%	38%
C(³ P)+O(¹ D)	-	9.4%	-	8%	-	15%	-	11%
C(¹ D)+O(³ P)	13.41%	14.5%	19.15%	34%	9.61%	35%	4.50%	35%
C(¹ S)+O(³ P)		0.0%			10^{-5} %	5%	10^{-2} %	5%
C(¹ D)+O(¹ D)				5%	47.14%	6%	44.56%	11%
C(³ P)+O(¹ S)							$\sim 10^{-11}$ %	
C(¹ S)+O(¹ D)		-		-		-	$\sim 10^{-7}$ %	-

[†] [1]

interaction between the closed channels, associated with higher vibrational ion levels and the current dissociative states, contaminates, via non-adiabatic or indirect electronic coupling, the direct interaction between the entrance and the dissociative channels. This results in a stronger capture probability, and consequently a higher DR cross section, which leads to the rich resonance structures observed in the total cross section. The direct DR cross section is proportional to the square of the Franck-Condon overlap, of the type seen in Eq. (5), between the vibrational wave functions of the ion and the dissociation state of the neutral. The favorable crossings at lower collision energies of the dissociation states correlating to the C(³P)+O(³P) and C(¹D)+O(¹D) atomic limits (blue and cyan curves in Fig. 2) with the ionic ground state (black curve on the same figure) and the significant couplings to the entrance channel are responsible for the large contribution by the direct DR cross sections to all the three symmetries used in the calculations. This is the smooth background cross section on which the contribution from the indirect process is superimposed, resulting in the total cross section shown in Fig. 4. The closed ionization channels are those responsible for the temporary capture into the Rydberg states and consequently to the indirect mechanism. There is an increasing number of resonance states of all symmetries at higher energies, and some or all of these can participate in the DR process via channel mixing mechanism.

The role of each dissociation channel depends on the energy of the incident electron. At higher collision energies, when the other two dissociation channels become open (magenta and red curves in figure 2) due to their less-favorable crossings with the ionic ground state the indirect process gains importance leading to the resonance structures in the total cross section. We have included all the contributions of the dissociative channels in our calculations.

In view of the comparison with the storage-ring measurements, we have convoluted our MQDT cross sections with the *anisotropic* Maxwell velocity distribution function for the electrons. The transversal and longitudinal temperatures are $K_B T_{\perp} = 1$ meV and $K_B T_{\parallel} = 10$ meV, respectively. The calculated anisotropic rate coefficient (magenta) together with the measured one (green) [1] are shown in figure 5. The overall agreement with exper-

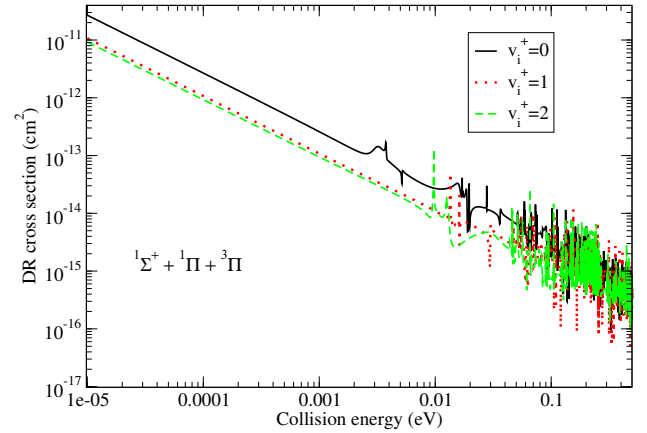


FIG. 7: Total DR cross sections for different initial vibrational levels of the ion, for all the considered symmetries. Black continuous line stand for $v_i^+ = 0$, while the red dotted and green dashed lines for $v_i^+ = 1$ and 2, respectively.

imental value is good, our calculated rate coefficient reproduces perfectly the trends of the experimental curves, underestimating them on average by a factor of 2.

In addition to the anisotropic rate coefficients, starting from the computed cross section, we have evaluated the Maxwell *isotropic* rate coefficient as well, for a broad range of electronic temperatures, relevant especially for cold non-equilibrium plasmas. The rate for $v_i^+ = 0$ is displayed in figure 6, and its thermal (300 K) value is in excellent agreement with the measured values obtained in merged-beam [9] and [49] as well as storage-ring based [1] collision experiments. The rate coefficients of [48] presented as red circles in the figure are placed higher than the other measurements, probably due to the presence of $\text{CO}^+ \cdot (\text{CO})_n$ clusters in the sample, as it was pointed out by [50]. Moreover, our calculations have shown much less isotopic effect than those found by [13], having as mean deviation 0.43% (due to the different nuclear reduced masses) among the two isotopologues.

Finally, we have calculated dissociative recombination, vibrational excitation (VE) and de-excitation (VdE) cross sections for different vibrational levels in the entrance channels, namely for $v_i^+ = 1$ and 2 and compared with

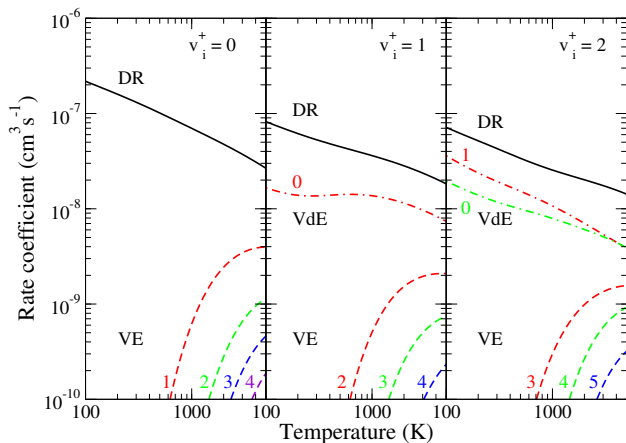


FIG. 8: DR and state-to-state VE and VdE isotropic rate coefficients of CO^+ in its ground electronic state, v_i^+ standing for the vibrational quantum number of the target ion. Curves of same color show the rate coefficients for the vibrational (de-)excitations corresponding to the same $|\Delta v| = |v_f^+ - v_i^+|$, $v_f > v_i$ for the VE and $v_f < v_i$ for the VdE global rate coefficients, respectively. The final vibrational quantum numbers of the ion are indicated for these processes.

the cross sections found for $v_i^+ = 0$. The comparison of the DR cross sections can be seen in figure 7. We find that the DR cross section for the ground vibrational levels exceeds significantly, by more than a factor of 2, those of $v_i^+ = 1$ and 2, whereas the later ones have similar rates.

Figure 8 shows the total DR and vibrational transition (VE, VdE) rate coefficients for the three initial vibrational levels of the ion. We find the highest rates for all the processes for $v_i^+ = 0$, their magnitude decreases with excitation of the initial ionic vibrational level, except for the $\Delta v = v_f^+ - v_i^+ = -1$ de-excitation transitions where the $v_i^+ = 2$ gives higher rates.

The trends of the observables are the same for both the cross section and rate coefficients. Thus one can conclude that whenever the initial sample can contain ions with excited vibrational levels, fully accounting for them will be important.

To aid the simple use of the rate coefficients shown in Fig. 8, we have fitted them using simple formulas. The calculated DR rate coefficients for $\text{CO}^+(v = 0, 1, 2)$ is represented by:

$$k_{(\text{CO}^+),v}^{\text{DR}}(T_e) = A_v T_e^{\alpha_v} \exp \left[- \sum_{i=1}^7 \frac{B_v(i)}{i T_e^i} \right] \quad (17)$$

over the electron temperature range $T_{\min} < T_e < 5000$ K with $T_{\min} = 100$ K. The values given by Eq. (17) depart from the reference values by only a few percent. The parameters A_v , α_v and $B_v(i)$ are listed in Table II. The corresponding formula for the vibrational transitions (VE and VdE) has the form:

$$k_{(\text{CO}^+),v' \rightarrow v''}^{\text{VE,VdE}}(T_e) = A_{v' \rightarrow v''} T_e^{\alpha_{v' \rightarrow v''}} \exp \left[- \sum_{i=1}^7 \frac{B_{v' \rightarrow v''}(i)}{i T_e^i} \right] \quad (18)$$

over the electron temperature range $T_{\min} < T_e < 5000$ K. Again the values calculated using Eq. (18) depart from the referenced values only by a few percent. The parameters T_{\min} , $A_{v' \rightarrow v''}$, $\alpha_{v' \rightarrow v''}$ and the different $B_{v' \rightarrow v''}(i)$ for $i \in [1, 7]$ are listed in Tables III to V.

VI. CONCLUSION

This paper presents a theoretical study of DR of CO^+ over a broad range of electron energies including several dissociation states with different symmetries. Although our basic approach is *ab initio*, using such methods it is not yet possible to compute the position of the dissociative curves involved in the DR process accurately enough to give reliable results. We have therefore used potential curves derived from spectroscopic data on CO to calibrate the *ab initio* data. Our DR calculations using these calibrated curves give good agreement with the low-energy experimental data, up to about 3 eV, significantly improving the results of existing previous studies. We note however the very recent study of DR N_2^+ performed by [51] based on fully *ab initio* potential energy curves and couplings computed with the R-matrix method [52, 53]. N_2^+ is isoelectronic with CO^+ , although its higher symmetry makes it somewhat easier to treat. These studies suggest that a similar, accurate, fully *ab initio* treatment of the CO^+ problem should be possible in the fairly near future.

A major motivation of this paper was to show and test the applicability of our method, whenever there are significant lacks of reliable quantum chemistry calculations. We have performed calculations making use of 4 dissociation states in three different symmetry accounting Rydberg states up to four partial waves. The calculations were done in the highest order of complexity possible.

On overall, one can say that the agreement achieved between theory and experiment over a significant range of energies is satisfactory, the trends being qualitatively reproduced for this diatomic system with many-electrons. This suggests that our calibrated *ab initio* approach provides a suitable procedure for studying other many-electron systems for which pure *ab initio* calculations are not reliable.

The found results are of fundamental importance and very promising, suggesting for a need of further studies especially for improved and more accurate potential energy curves and couplings not just for the molecular ion but for neutral molecule as well.

Acknowledgments

The authors thank Ch. Jungen and S. L. Guberman for numerous and fruitful discussions. They acknowledge support from the International Atomic Energy Agency via the Coordinated Research Project "Light Element Atom, Molecule and Radical Behaviour in the Divertor and Edge Plasma Regions," from Agence Nationale de la Recherche via the projects "SUMOSTAI" (No. ANR-09-BLAN-020901) and "HYDRIDES" (No.

TABLE II: Parameters used in Eq. (17) to represent the DR rate coefficients of CO^+ .

v	A_v	α_v	$B_v(1)$	$B_v(2)$	$B_v(3)$	$B_v(4)$	$B_v(5)$	$B_v(6)$	$B_v(7)$
0	$.281949503 \times 10^{-04}$	$-.802579890 \times 10^{00}$	$.710130957 \times 10^{03}$	$-.698308895 \times 10^{06}$	$.335177615 \times 10^{09}$	$-.850620477 \times 10^{11}$	$.117104453 \times 10^{14}$	$-.826280436 \times 10^{15}$	$.233919918 \times 10^{17}$
1	$.715701893 \times 10^{-05}$	$-.682706983 \times 10^{00}$	$.843520677 \times 10^{03}$	$-.713971932 \times 10^{06}$	$.300490272 \times 10^{09}$	$-.703053442 \times 10^{11}$	$.920945293 \times 10^{13}$	$-.629626035 \times 10^{15}$	$.174554736 \times 10^{17}$
2	$.158116294 \times 10^{-05}$	$-.537454517 \times 10^{00}$	$.740102970 \times 10^{03}$	$-.910764930 \times 10^{06}$	$.460910057 \times 10^{09}$	$-.118698360 \times 10^{12}$	$.163967837 \times 10^{14}$	$-.115670469 \times 10^{16}$	$.327041619 \times 10^{17}$

TABLE III: Parameters used in Eq. (18) to represent the VE rate coefficients of CO^+ ($v' = 0$).

$v' \rightarrow v''$	$T_{min}(K)$	$A_{v' \rightarrow v''}$	$\alpha_{v' \rightarrow v''}$	$B_{v' \rightarrow v''}(1)$	$B_{v' \rightarrow v''}(2)$	$B_{v' \rightarrow v''}(3)$	$B_{v' \rightarrow v''}(4)$	$B_{v' \rightarrow v''}(5)$	$B_{v' \rightarrow v''}(6)$	$B_{v' \rightarrow v''}(7)$
0 \rightarrow 1	100	$.641552103 \times 10^{-05}$	$-.771371374 \times 10^{00}$	$.414475403 \times 10^{04}$	$-.555697606 \times 10^{06}$	$.177113555 \times 10^{09}$	$-.379319033 \times 10^{11}$	$.499340108 \times 10^{13}$	$-.353310994 \times 10^{15}$	$.101763661 \times 10^{17}$
0 \rightarrow 2	200	$.748711072 \times 10^{-05}$	$-.848613994 \times 10^{00}$	$.808028559 \times 10^{04}$	$-.314102151 \times 10^{07}$	$.267788469 \times 10^{10}$	$-.125332604 \times 10^{13}$	$.323013435 \times 10^{15}$	$-.429933877 \times 10^{17}$	$.230779467 \times 10^{19}$
0 \rightarrow 3	250	$.653782258 \times 10^{-05}$	$-.889871881 \times 10^{00}$	$.100400799 \times 10^{05}$	$-.153427057 \times 10^{07}$	$.166204703 \times 10^{10}$	$-.968343280 \times 10^{12}$	$.307963790 \times 10^{15}$	$-.505267521 \times 10^{17}$	$.334692067 \times 10^{19}$
0 \rightarrow 4	300	$.410991022 \times 10^{-04}$	$-.111309015 \times 10^{01}$	$.144578277 \times 10^{05}$	$-.425122442 \times 10^{07}$	$.457572230 \times 10^{10}$	$-.279947663 \times 10^{13}$	$.974452298 \times 10^{15}$	$-.180068315 \times 10^{18}$	$.137000155 \times 10^{20}$
0 \rightarrow 5	350	$.673816604 \times 10^{-04}$	$-.121225593 \times 10^{01}$	$.186129714 \times 10^{05}$	$-.751669966 \times 10^{07}$	$.865504846 \times 10^{10}$	$-.581314625 \times 10^{13}$	$.227948002 \times 10^{16}$	$-.482391689 \times 10^{18}$	$.424701037 \times 10^{20}$
0 \rightarrow 6	400	$.678304142 \times 10^{-04}$	$-.126655170 \times 10^{01}$	$.216968564 \times 10^{05}$	$-.932715458 \times 10^{07}$	$.125788319 \times 10^{11}$	$-.980812594 \times 10^{13}$	$.440562841 \times 10^{16}$	$-.105632400 \times 10^{19}$	$.104556888 \times 10^{21}$
0 \rightarrow 7	450	$.935214058 \times 10^{-04}$	$-.135011215 \times 10^{01}$	$.242759946 \times 10^{05}$	$-.866103794 \times 10^{07}$	$.131034124 \times 10^{11}$	$-.117137348 \times 10^{14}$	$.603374022 \times 10^{16}$	$-.165375862 \times 10^{19}$	$.186623905 \times 10^{21}$
0 \rightarrow 8	500	$.127223673 \times 10^{-03}$	$-.143309661 \times 10^{01}$	$.268650737 \times 10^{05}$	$-.655138124 \times 10^{07}$	$.888503051 \times 10^{10}$	$-.729741009 \times 10^{13}$	$.338502966 \times 10^{16}$	$-.803004985 \times 10^{18}$	$.732964756 \times 10^{20}$
0 \rightarrow 9	550	$.106418750 \times 10^{-03}$	$-.146917756 \times 10^{01}$	$.289593294 \times 10^{05}$	$-.336743387 \times 10^{07}$	$.171303281 \times 10^{10}$	$-.296792983 \times 10^{13}$	$.156774183 \times 10^{16}$	$-.292893172 \times 10^{21}$	
0 \rightarrow 10	600	$.1443000838 \times 10^{-04}$	$-.135396575 \times 10^{01}$	$.296834933 \times 10^{05}$	$-.806531715 \times 10^{07}$	$.280264726 \times 10^{11}$	$-.444214735 \times 10^{14}$	$-.379357647 \times 10^{17}$	$.167825913 \times 10^{20}$	$-.301076067 \times 10^{22}$
0 \rightarrow 11	650	$.867766831 \times 10^{-07}$	$-.958697496 \times 10^{00}$	$.257440709 \times 10^{05}$	$.409137189 \times 10^{08}$	$-.119011764 \times 10^{12}$	$-.170031924 \times 10^{15}$	$.799092375 \times 10^{20}$	$-.152981923 \times 10^{23}$	
0 \rightarrow 12	700	$.325017591 \times 10^{-32}$	$.446113412 \times 10^{01}$	$-.512283310 \times 10^{05}$	$.493759852 \times 10^{09}$	$-.147156377 \times 10^{13}$	$-.246380214 \times 10^{16}$	$-.2329888126 \times 10^{19}$	$.115912196 \times 10^{22}$	$-.235418187 \times 10^{24}$

TABLE IV: Parameters used in Eq. (18) to represent the VE and VdE rate coefficients of CO⁺ ($v' = 1$).

$v' \rightarrow v''$	T_{min}	$A_{v' \rightarrow v''}$	$\alpha_{v' \rightarrow v''}$	$B_{v' \rightarrow v''}(1)$	$B_{v' \rightarrow v''}(2)$	$B_{v' \rightarrow v''}(3)$	$B_{v' \rightarrow v''}(4)$	$B_{v' \rightarrow v''}(5)$	$B_{v' \rightarrow v''}(6)$	$B_{v' \rightarrow v''}(7)$
1 → 0	100	633920326 × 10 ⁻⁰⁵	-770044378 × 10 ⁰⁰	104178437 × 10 ⁰⁴	-551232678 × 10 ⁰⁶	175018067 × 10 ⁰⁹	-374062491 × 10 ¹¹	492117834 × 10 ¹³	-348198826 × 10 ¹⁵	100308337 × 10 ¹⁷
1 → 2	100	112757539 × 10 ⁻⁰⁵	-667253557 × 10 ⁰⁰	301658328 × 10 ⁰⁴	265128201 × 10 ⁰⁶	-167485020 × 10 ⁰⁹	460282036 × 10 ¹¹	-652022601 × 10 ¹³	465696778 × 10 ¹⁵	-132656980 × 10 ¹⁷
1 → 3	150	562989138 × 10 ⁻⁰⁶	-651039420 × 10 ⁰⁰	526482012 × 10 ⁰⁴	134397812 × 10 ⁰⁷	-848709209 × 10 ⁰⁹	288214188 × 10 ¹²	-547449693 × 10 ¹⁴	544047009 × 10 ¹⁶	-219710957 × 10 ¹⁸
1 → 4	200	130991873 × 10 ⁻⁰⁶	-537069718 × 10 ⁰⁰	875368149 × 10 ⁰⁴	339794737 × 10 ⁰⁶	-146345601 × 10 ⁰⁹	270246030 × 10 ¹¹	-183890443 × 10 ¹²	736617748 × 10 ¹⁵	699602764 × 10 ¹⁷
1 → 5	250	209439988 × 10 ⁻⁰⁵	-858043793 × 10 ⁰⁰	147483446 × 10 ⁰⁵	-617683461 × 10 ⁰⁷	628994423 × 10 ¹⁰	-343234925 × 10 ¹³	103740710 × 10 ¹⁶	-163563141 × 10 ¹⁸	104899664 × 10 ²⁰
1 → 6	300	439087022 × 10 ⁻⁰⁵	-950117793 × 10 ⁰⁰	180805100 × 10 ⁰⁵	-780708040 × 10 ⁰⁷	975729438 × 10 ¹⁰	-654274154 × 10 ¹³	239495154 × 10 ¹⁶	-451595265 × 10 ¹⁸	342947398 × 10 ²⁰
1 → 7	350	990587644 × 10 ⁻⁰⁵	-107079534 × 10 ⁰¹	209321916 × 10 ⁰⁵	-904877766 × 10 ⁰⁷	124117280 × 10 ¹¹	-929195541 × 10 ¹³	387627434 × 10 ¹⁶	-844294279 × 10 ¹⁸	746823381 × 10 ²⁰
1 → 8	400	290364496 × 10 ⁻⁰⁵	-976365340 × 10 ⁰⁰	209545755 × 10 ⁰⁵	435177075 × 10 ⁰⁷	-136200658 × 10 ¹¹	175763114 × 10 ¹⁴	-114936867 × 10 ¹⁷	372696383 × 10 ¹⁹	-475130034 × 10 ²¹
1 → 9	450	553151534 × 10 ⁻⁰⁵	-107588250 × 10 ⁰¹	228931552 × 10 ⁰⁵	102630980 × 10 ⁰⁸	-292944159 × 10 ¹¹	393966744 × 10 ¹⁴	-277151718 × 10 ¹⁷	982366990 × 10 ¹⁹	-138325077 × 10 ²²
1 → 10	500	295872921 × 10 ⁻¹⁸	190367144 × 10 ⁰¹	-111794851 × 10 ⁰⁵	184960763 × 10 ⁰⁹	-439761036 × 10 ¹²	564818219 × 10 ¹⁵	-399526307 × 10 ¹⁸	146086706 × 10 ²¹	-215320891 × 10 ²³
1 → 11	550	860719793 × 10 ⁻¹⁴	818099637 × 10 ⁰⁰	202216367 × 10 ⁰⁴	144200890 × 10 ⁰⁹	-371106005 × 10 ¹²	518902243 × 10 ¹⁵	-402326107 × 10 ¹⁸	162115803 × 10 ²¹	-264323393 × 10 ²³
1 → 12	600	238429782 × 10 ⁻²⁴	309243990 × 10 ⁰¹	-287784203 × 10 ⁰⁵	327916264 × 10 ⁰⁹	-895346410 × 10 ¹²	135575406 × 10 ¹⁶	-114959696 × 10 ¹⁹	509491570 × 10 ²¹	-917135223 × 10 ²³
1 → 13	650	171475246 × 10 ⁻⁵³	946512823 × 10 ⁰¹	-118535342 × 10 ⁰⁶	845804438 × 10 ⁰⁹	-241202045 × 10 ¹³	384508952 × 10 ¹⁶	-344818061 × 10 ¹⁹	162171803 × 10 ²²	-310615978 × 10 ²⁴

TABLE V: Parameters used in Eq. (18) to represent the VE and VdE rate coefficients of CO⁺ ($v' = 2$).

$v' \rightarrow v''$	T_{min}	$A_{v' \rightarrow v''}$	$\alpha_{v' \rightarrow v''}$	$B_{v' \rightarrow v''}(1)$	$B_{v' \rightarrow v''}(2)$	$B_{v' \rightarrow v''}(3)$	$B_{v' \rightarrow v''}(4)$	$B_{v' \rightarrow v''}(5)$	$B_{v' \rightarrow v''}(6)$	$B_{v' \rightarrow v''}(7)$
2 → 0	100	143264325 × 10 ⁻⁰⁵	-676398119 × 10 ⁰⁰	770399508 × 10 ⁰³	-649235829 × 10 ⁰⁶	280763127 × 10 ⁰⁹	-687619887 × 10 ¹¹	943978108 × 10 ¹³	-672803202 × 10 ¹⁵	193189057 × 10 ¹⁷
2 → 1	100	110150559 × 10 ⁻⁰⁵	-664642895 × 10 ⁰⁰	-475690563 × 10 ⁰²	274737488 × 10 ⁰⁶	-172309109 × 10 ⁰⁹	472936617 × 10 ¹¹	-669923671 × 10 ¹³	478615271 × 10 ¹⁵	-136383154 × 10 ¹⁷
2 → 3	100	296299450 × 10 ⁻⁰⁶	-540421763 × 10 ⁰⁰	322902717 × 10 ⁰⁴	-185353201 × 10 ⁰⁶	102324472 × 10 ⁰⁹	-295771623 × 10 ¹¹	446770807 × 10 ¹³	-336457775 × 10 ¹⁵	998160611 × 10 ¹⁶
2 → 4	150	278155705 × 10 ⁻⁰⁵	-783269363 × 10 ⁰⁰	680722101 × 10 ⁰⁴	-103878379 × 10 ⁰⁷	741843999 × 10 ⁰⁹	-276056904 × 10 ¹²	549666157 × 10 ¹⁴	-558745281 × 10 ¹⁶	228035409 × 10 ¹⁸
2 → 5	200	266683567 × 10 ⁻⁰⁴	-107862034 × 10 ⁰¹	110175934 × 10 ⁰⁵	-322418905 × 10 ⁰⁷	245112696 × 10 ¹⁰	-101947642 × 10 ¹³	237960237 × 10 ¹⁵	-292641709 × 10 ¹⁷	147503229 × 10 ¹⁹
2 → 6	250	542147000 × 10 ⁻⁰⁵	-983012338 × 10 ⁰⁰	122608040 × 10 ⁰⁵	321533385 × 10 ⁰⁶	-729487979 × 10 ⁰⁹	465646557 × 10 ¹²	-147373795 × 10 ¹⁵	236308026 × 10 ¹⁷	-153015638 × 10 ¹⁹
2 → 7	300	317786833 × 10 ⁻⁰⁶	-721222477 × 10 ⁰⁰	142487517 × 10 ⁰⁵	102722134 × 10 ⁰⁷	-582000169 × 10 ⁰⁹	484888182 × 10 ¹¹	644040556 × 10 ¹⁴	-223384907 × 10 ¹⁷	220068495 × 10 ¹⁹
2 → 8	350	273643357 × 10 ⁻⁰⁶	-744726391 × 10 ⁰⁰	184645633 × 10 ⁰⁵	-445860723 × 10 ⁰⁷	783952518 × 10 ¹⁰	-677237281 × 10 ¹³	310300559 × 10 ¹⁶	-723338935 × 10 ¹⁸	674944000 × 10 ²⁰
2 → 9	400	161814112 × 10 ⁻⁰⁵	-947134778 × 10 ⁰⁰	222431469 × 10 ⁰⁵	-163473342 × 10 ⁰⁷	438401719 × 10 ¹⁰	980397656 × 10 ¹³	-775362755 × 10 ¹⁶	276484946 × 10 ¹⁹	-372814588 × 10 ²¹
2 → 10	450	857949106 × 10 ⁻⁰⁵	-113992880 × 10 ⁰¹	247605739 × 10 ⁰⁵	513853850 × 10 ⁰⁷	-233874625 × 10 ¹¹	348626787 × 10 ¹⁴	-254552925 × 10 ¹⁷	917457255 × 10 ¹⁹	-130303783 × 10 ²²
2 → 11	500	222319239 × 10 ⁻¹¹	337546441 × 10 ⁰⁰	802866148 × 10 ⁰⁴	966824466 × 10 ⁰⁸	-237713634 × 10 ¹²	308999968 × 10 ¹⁵	-219586955 × 10 ¹⁸	804421605 × 10 ²⁰	-118654044 × 10 ²³
2 → 12	550	967268411 × 10 ⁻¹¹	141405228 × 10 ⁰⁰	108888796 × 10 ⁰⁵	100995726 × 10 ⁰⁹	-264030143 × 10 ¹²	370381461 × 10 ¹⁵	-287172365 × 10 ¹⁸	115625983 × 10 ²¹	-188366916 × 10 ²³
2 → 13	600	859235026 × 10 ⁻¹¹	675737504 × 10 ⁻⁰¹	117098302 × 10 ⁰⁵	110881879 × 10 ⁰⁹	-305068188 × 10 ¹²	463253664 × 10 ¹⁵	-392591768 × 10 ¹⁸	173889056 × 10 ²¹	-312870721 × 10 ²³
2 → 14	650	164458016 × 10 ⁻²³	280896167 × 10 ⁰¹	-257956296 × 10 ⁰⁵	332078837 × 10 ⁰⁹	-946887885 × 10 ¹²	150871571 × 10 ¹⁶	-135222037 × 10 ¹⁹	635505472 × 10 ²¹	-121648562 × 10 ²⁴

ANR-12-BS05-0011-01), from the IFRAF-Triangle de la Physique via the project "SpecoRyd," and from the Centre National de la Recherche Scientifique via the programs "Physique et Chimie du Milieu Interstellaire," and the PEPS projects "Physique théorique et ses interfaces" TheMS and TPCECAM. They also acknowledge generous financial support from La Région Haute-Normandie via the CPER "THETE" project, and the GRR Electronique, Energie et Matriaux, from the "Fédération de Recherche Energie, Propulsion, Environnement," and from the LabEx EMC³, via the project PicoLIBS (No. ANR-10-LABX-09-01). K.C. thanks the department In-

stitut des Sciences de l'Ingénierie et des Systèmes (INSIS) of CNRS for a research grant in 2013, and Laboratoire Ondes et Milieux Complexes (LOMC) of Le Havre University for hospitality.

Data availability

Upon a reasonable request, the data supporting this article will be provided by the corresponding author.

-
- [1] Rosen S, Peverall R, Larson M, Le Padellec A, Semaniak J, Larson Å, Strömholm C, Zande W J Vn der, Danared H and Dunn G H 1998 *Phys. Rev. A* **57**, 4462.
- [2] Chakrabarti K and Tennyson J 2006 *J. Phys. B: At. Mol. Opt. Phys.* **39**, 1485.
- [3] Chakrabarti K and Tennyson J 2007 *J. Phys. B: At. Mol. Opt. Phys.* **40**, 2135.
- [4] Eidelsberg M, Lemaire J L, Federman S R, Stark G, Heays A N, Sheffer Y, Gavilan L, Fillion J H, Rostas F, Lyons J R, Smith P L, de Oliveira N, Joyeux D, Roudjane M and Nahon L 2012 *Astronomy & Astrophysics* **543**, A69.
- [5] Fowler A 1909 *Month. Not. R: Astr. Soc.* **70**, 176.
- [6] Fuente A, Garcia-Burillo S, Gerin M, Rizzo J R, Usero A, Teyssier D, Roueff E and le Bourlot J 2010 *Astrophys. J* **641**, L105.
- [7] Krupente P H and Weissman S 1965 *J. Chem. Phys.* **43**, 1529.
- [8] Seaton M. J. 1966 *Proc. Phys. Soc. (London)* **88**, 801.
- [9] Mitchell J B A and Hus H 1985 *J. Phys. B: At. Mol. Phys.* **18**, 547.
- [10] Park C *et al* 1994 *J. Thermophys. Heat Transfer* **8**, 9.
- [11] Bultel A, Chéron B G, Bourdon A, Motapon O and Schneider I F 2006 *Phys. Plasmas* **13**, 043502.
- [12] Fox J L 1999 *Bull. Am. Astron. Soc.* **31**, 1584.
- [13] Guberman S L 2007, *Workshop on Planetary Atmospheres*, communication.
- [14] Geoghegan M, Adams N G and Smith D 1991 *J. Phys. B* **24**, 2589.
- [15] Giusti-Suzor A 1980 *J. Phys. B: At. Mol. Phys.* **13**, 3867.
- [16] Seaton M J 1983 *Rept. Prog. Phys.* **46**, 167.
- [17] Greene C H and Jungen Ch 1985 *Adv. At. Mol. Phys.* **21**, 51.
- [18] Jungen C 1996, ed., *Molecular Applications of Quantum Defect Theory*, Institute of Physics Publishing Bristol.
- [19] Giusti-Suzor A, Bardsley J. N and Derkits C 1983 *Phys. Rev. A* **28**, 682.
- [20] Schneider I F, Dulieu O and Giusti-Suzor A 1991 *J. Phys. B: At. Mol. Phys.* **24**, L289.
- [21] Takagi H 1993 *J. Phys. B: At. Mol. Opt. Phys.* **26**, 4815.
- [22] Tanabe T, Katayama I, Kamegaya H, Chida K, Arakaki Y, Watanabe T, Yoshizawa M, Saito M, Haruyama Y, Hosono K, Hatanaka K, Honma T, Noda K, Ohtani S and Takagi H 1995 *Phys. Rev. Lett.* **75**, 1066.
- [23] Schneider I F, Strömholm C, Carata L, Urbain X, Larsson M and Suzor-Weiner A 1997 *J. Phys. B: At. Mol. Opt. Phys.* **30**, 2687.
- [24] Amitay Z, Baer A, Dahan M, Levin J, Vager Z, Zajfman D, Knoll L, Lange M, Schwalm D, Wester R, Wolf A, Schneider I F, and Suzor-Weiner A 1999 *Phys. Rev. A* **60**, 3769.
- [25] Guberman S L and Giusti-Suzor A 1991 *J. Chem. Phys.* **95**, 2602.
- [26] Guberman S L 2000 in M Larsson, J B A Mitchell and I F Schneider, eds., *Dissociative Recombination: Theory, Experiment and Applications IV*, World Scientific Singapore p. 111.
- [27] Sun H and Nakamura H 1990 *J. Chem. Phys.* **93**, 6491.
- [28] Vălcu B, Schneider I F, Raoult M, Strömholm C, Larsson M and Suzor-Weiner A 1998 *European Physical Journal D* **1**, 71.
- [29] Schneider I F, Rabadán, Carata L, Andersen L H, Suzor-Weiner A and Tennyson J 2000a *J. Phys. B: At. Mol. Opt. Phys.* **33**, 4849.
- [30] Schneider I F, Orel A E and Suzor-Weiner A 2000b *Phys. Rev. Lett.* **85**, 3785.
- [31] Kokouline V, Greene C H and Esry B D 2001 *Nature* **412**, 891.
- [32] Kokouline V and Greene C H 2003 *Phys. Rev. A* **68**, 012703.
- [33] Ngassam V, Motapon O, Florescu A, Pichl L, Schneider I F and Suzor-Weiner A 2003a *Phys. Rev. A* **68**, 032704.
- [34] Motapon O, Fifirig M, Florescu A, Waffeu Tamo F O, Crumeyrolle O, Varin-Bréant G, Bultel A, Vervisch P, Tennyson J and Schneider I F, 2006 *Plasma Sources Sci. Technol.* **15**, 23.
- [35] Faure A and Tennyson J 2001 *Month. Not. R: Astr. Soc.* **325**, 443.
- [36] Sidis V and Lefebvre-Brion H 1971 *J. Phys. B* **4**, 1040.
- [37] Jungen C and Atabek O 1977 *J. Chem. Phys.* **66**, 5584.
- [38] Ngassam V, Florescu A, Pichl L, Schneider I F, Motapon O, and Suzor-Weiner A 2003b *Eur. Phys. J. D* **26**, 165.
- [39] Tennyson J 1996a *J. Phys. B: At. Mol. Opt. Phys.* **29**, 1817.
- [40] Tennyson J 1996b *J. Phys. B: At. Mol. Opt. Phys.* **29**, 6185.
- [41] Tchang-Brillet W-Ü L., Julianne P S, Robbe J-M, Letzelter C and Rostas F 1992 *J. Chem. Phys.* **96**, 6735.
- [42] Lefebvre-Brion H and Lewis B R 2007 *Mol. Phys.* **105**, 1625.
- [43] Vázquez G J, Amero J M, Liebermann H P and Lefebvre-Brion H 2009 *J. Chem. Phys.* **113**, 13395.
- [44] Lefebvre-Brion H, Liebermann H P and Vázquez G J 2010 *J. Chem. Phys.* **132**, 024311.
- [45] Wigner E and Witmer E E 1928 *Z. Physik* **51**, 859.
- [46] Pichl L, Nakamura H and Horacek J 2000 *CPC* **124**, 1.
- [47] Takagi H 2000 in M Larsson, J B A. Mitchell and I F Schneider, eds., *Dissociative Recombination: Theory, Ex-*

- periment and Applications IV* World Scientific Singapore p. 180.
- [48] Mentzoni M H and Donohoe J 1968 *Phys. Lett.* **26A**, 330.
- [49] Laubé S, Lehfaoui L, Rowe B R and Mitchell J B A 1998 *J. Phys. B: At. Mol. Opt. Phys.* **31**, 4181.
- [50] Whitaker M, Biondi M A, and Johnsen R 1981 *Phys. Rev. A* **23**, 1481.
- [51] Little D A, Chakrabarti K, Mezei J Zs, Schneider I F, and Tennyson J 2014*b* *Phys. Rev. A* **90**, 052705.
- [52] Little D A and Tennyson J 2013 *J. Phys. B: At. Mol. Opt. Phys.* **46**, 145102.
- [53] Little D A and Tennyson J 2014*a* *J. Phys. B: At. Mol. Opt. Phys.* **47**, 105204.